JOURNAL OF MATERIALS SCIENCE 37 (2002) 4419–4424

Effect of atmosphere on superplastic deformation behavior in nanocrystalline liquid-phase-sintered silicon carbide with Al_2O_3-Y_2O_3 additions

T. NAGANO, H. GU
Ceramics Superplasticity Project, ICORP, Japan Science and Technology Corporation, Nagoya 456-8587, Japan

G.-D. ZHAN
Department of Chemical Engineering and Materials Science, University of California 95616, Davis, USA

M. MITOMO
National Institute for Materials Science, Tsukuba 305-0044, Japan

Nanocrystalline β-SiC with additions of 5.135 wt% Al_2O_3 and 3.867 wt% Y_2O_3 was subjected to tensile deformation in order to study its microstructural behavior under the dynamic process. The liquid-phase-sintered body had a relative density of >95% and an average grain size of 190 nm. Tension tests were conducted at initial strain rates range from 3×10^{-4} to 2×10^{-5} s^{-1}, in the temperature range 1873–2048 K, in both argon and N_2 atmospheres. Although grain-boundary liquids formed by the additions vaporized concurrently with the decomposition of SiC and grain growth, the maximum tensile elongation of 60% was achieved in argon. The grain-boundary amorphous phase formed a crystalline phase during testing in an N_2 atmosphere and fracture occurred at <8% elongation. Grain-boundary sliding was still the dominant mechanism for deformation.

1. Introduction

Silicon carbide (SiC) is difficult to densify without sintering additives because of the covalent nature of the Si—C bonding and the low self-diffusion coefficient. SiC has attracted much attention as a structural material since Prochazka [1] reported on it in 1973. With boron and carbon as additives, Prochazka used pressureless sintering to fabricate dense SiC that maintained excellent strength up to 1773 K. The additives lowered the grain-boundary energy and promoted sintering. Superior mechanical strength at high temperature was achieved because the additives were incorporated into the SiC as a solid solution.

In liquid-phase sintering, Suzuki [2] fabricated a sintered body with a density of >97% of the theoretical value using β-SiC powder with Al_2O_3 as an additive. Omori and Takei [3] fabricated β-SiC with 96.8% of full density using Al_2O_3 and Y_2O_3 additives. The sintering temperatures of these liquid-phase-sintered materials were >2173 K, as high as those in Prochazka's solid-phase sintering, and phase transformation from isotropioc β grains to anisotropic α grains occurred during sintering.

Superplasticity is phenomenologically defined as the ability of a polycrystalline material to exhibit an extraordinary large elongation during tension testing. Ceramic superplasticity is generally exhibited in polycrystals with an average grain size of <1 μm.

Recently, dense nanocrystalline SiC with oxide additives was fabricated by hot pressing [4]. In liquid-phase-sintered β-SiC, an amorphous phase was observed at grain boundaries [5–7]. Liquid-phase-sintered SiC with an amorphous phase at the grain boundaries can be deformed at lower deformation temperatures, lower flow stresses, and higher strain rates in comparison with boron and carbon-doped SiC with no amorphous phase at the grain boundaries.

The superplastic deformation temperature of liquid-phase sintered β-SiC in argon (>1973 K) [5–9], however, was higher that of Si_3N_4 in N_2 (1873 K) [10]. Therefore, the vaporization of amorphous phase and grain growth during deformation prevented large elongation.

The authors of this study also investigated the effect of atmosphere on the weight loss of liquid-phase sintered β-SiC with oxide additives during the heat treatment, and found that the weight loss in N_2 was suppressed about 1/2 to 1/3 in comparison with the weight loss in Ar [11]. Jun and co-workers [12] compared the sintering behavior of SiC in both argon and N_2 atmospheres and reported that grain growth and phase transformation from β to α were suppressed in N_2.

Accordingly, deformation of SiC with an amorphous phase at high temperature is influenced by dynamic microstructural change and atmosphere during those tests.

For this study, the effect of atmosphere on deformation behavior and dynamic microstructural change of liquid-phase-sintered β-SiC with Al_2O_3 and Y_2O_3 was investigated in both argon and N_2 atmospheres.

2. Experimental procedure

The starting material was ultrafine β-SiC powder (T-1 grade, Sumitomo-Osaka Cement Co., Tokyo, Japan) fabricated by plasma-enhanced chemical vapor deposition. The average grain size was 90 nm. The raw powder included 3.27 wt% free carbon. Excess free carbon prevents densification during sintering, therefore, after the raw powders had been annealed in air at 873 K for 2 h, they were soaked in hot HF and HNO_3 solution for 1 h and then rinsed in deionized water, which reduced the carbon content to 1.27 wt%. The powder was mixed with 5.135 wt% Al_2O_3 (AKP-20 grade, Sumitomo Chemical Co., Tokyo, Japan), 3.867 wt% Y_2O_3 (99.9% pure, Shinetsu Chemical Co., Tokyo, Japan) in *n*-hexane, using a SiC ball mill. Sintering was performed by hot-pressing under 30 MPa pressure, at 2048 K, for 30 min in argon. The relative bulk density was more than 95%. The as-sintered body was cut with a diamond cutter and ground using a diamond wheel. Tensile samples were dog-bone shaped, with a rectangular cross section (1 mm × 0.8 mm) and a gauge length of 4.4 mm. The sample surfaces were mirror-polished with 6 μm diamond paste.

Tension tests were conducted using a universal testing machine with furnace at constant crosshead speeds, at initial strain rates from 3×10^{-4} to 2×10^{-5} s^{-1}, in the temperature range 1873–2048 K, in both argon and N_2 atmospheres. The specimen was gripped by chucking devices, which were made of sintered SiC with the additions of boron and carbon. The degree of sample deformation was measured from the displacement of the crosshead. The tensile direction was perpendicular to the hot-pressing direction.

The true strain, ε_t, is defined as

$$\varepsilon_t = \ln(l/l_0) \tag{1}$$

where l and l_0 are the deformed and the original gauge length, respectively.

Assuming homogeneous deformation, true stress, σ_t, can be calculated by the relationship,

$$\sigma_t = \frac{P}{A_0}\exp(\varepsilon_t) \tag{2}$$

where P is the applied load and A_0 the cross section of the original sample.

The samples were observed after deformation, using scanning electron microscopy on the polished and plasma-etched surface, with $CF_4 + O_2$ (8%) gas. The average grain size for the linear intercept length is defined as follow [13].

$$d_{av} = 1.776L \tag{3}$$

Here, d_{av} is the average grain size and L the linear intercept length.

X-ray analysis was also conducted, to detect phase transformation and crystallization of the grain-boundary phase. The polytype contents of SiC were calculated using the method described by Tanaka [14].

The as-sintered material was prepared by polishing and argon-ion-beam thinning for observation by transmission electron microscope (TEM). High-resolution TEM (HRTEM) observation was performed using a 200 kV TEM (EM002B, TOPCON, Tokyo, Japan) with a point-to-point resolution of 0.18 nm. The grain-boundary composition was analyzed by both electron energy loss spectroscopy (EELS) and energy dispersive X-ray spectroscopy (EDX) using a scanning transmission electron microscope (Model No. HB601UX, VG Microscopes, East Grinstead, UK) with a minimum probe size of 0.22 nm.

Thermogravimetry-differential thermal analysis (TG-DTA: STA409, NETZSCH, Waldkraiburg, Germany) was performed in argon atmosphere to study the behavior of grain-boundary phase during tension testing. The heating rate was 20 K/min.

3. Results

3.1. Mechanical behavior

The true stress-true strain curves at the initial strain rate of 5×10^{-5} s^{-1} in argon are shown in Fig. 1. Flow stress decreased with increasing temperature. The maximum tensile elongation of 60% was obtained at 1998 K.

The true stress-true strain curves at the initial strain rate of 5×10^{-5} s^{-1} in N_2 are shown in Fig. 2. Strain softening was observed in all experimental conditions. All specimens were fractured at <8% elongation in spite of maximum true stress about <10 MPa.

3.2. Microstructural observation

Microstructural change before and after the tension tests is shown in Fig. 3. The as-sintered body was composed of equiaxed, fine grains (Fig. 3a). The grains were fully wetted. In deformed specimen in argon, grain growth occurred, but no anisotropy was observed. The grain size at fracture (50% elongation) was 490 nm. The vaporization of the grain-boundary phase is visible in

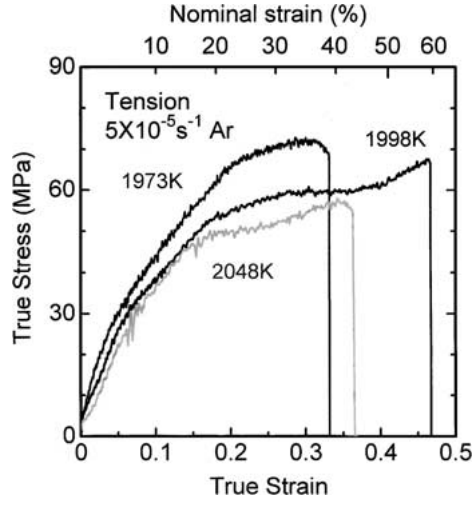

Figure 1 True stress-true strain curves at 5E-5 s^{-1} in Ar.

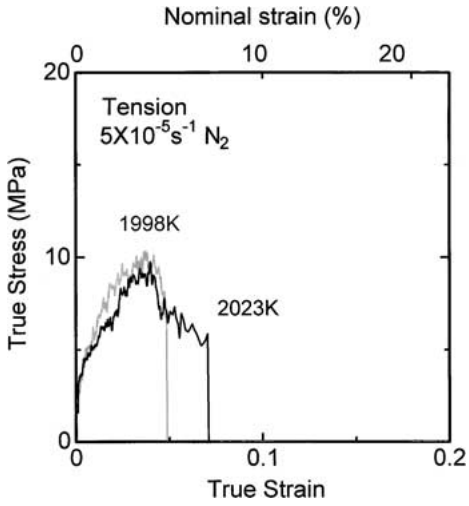

Figure 2 True stress-true strain curves at 5E-5 s^{-1} in N_2.

Fig. 3b. The submicron size of the cavities was also observed. On the other hand, in deformed specimen in N_2, the vaporization of grain-boundary phase was suppressed in comparison with that in argon (Fig. 3c). The grain size at fracture (7.3% elongation) was 360 nm. The cracks were propagated from sample surface into the inside of sample in the vertical direction of tensile axis (Fig. 3d).

An HRTEM image of the grain boundary in an as-sintered sample is shown in Fig. 4. An amorphous layer about 1 nm thick was evident at the grain boundary.

The energy-loss near-edge structure (ELNES) results for both grain and grain boundary before tension tests are shown in Fig. 5. The grain-boundary spectrum reveals that the amorphous layer contained aluminum, yttrium, and oxygen segregation those were not detected

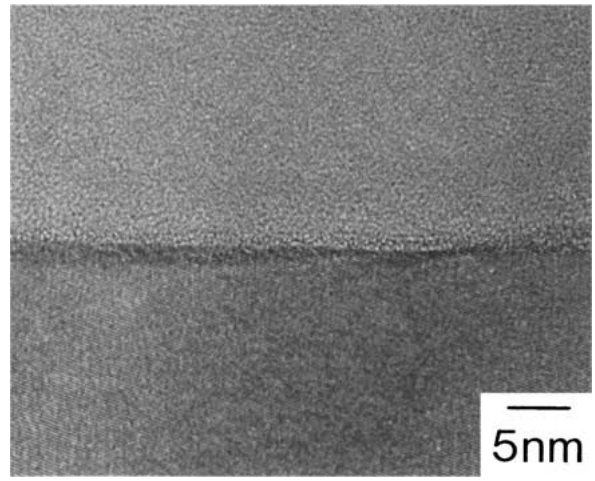

Figure 4 High-resolution TEM image at grain boundary in as-sintered material.

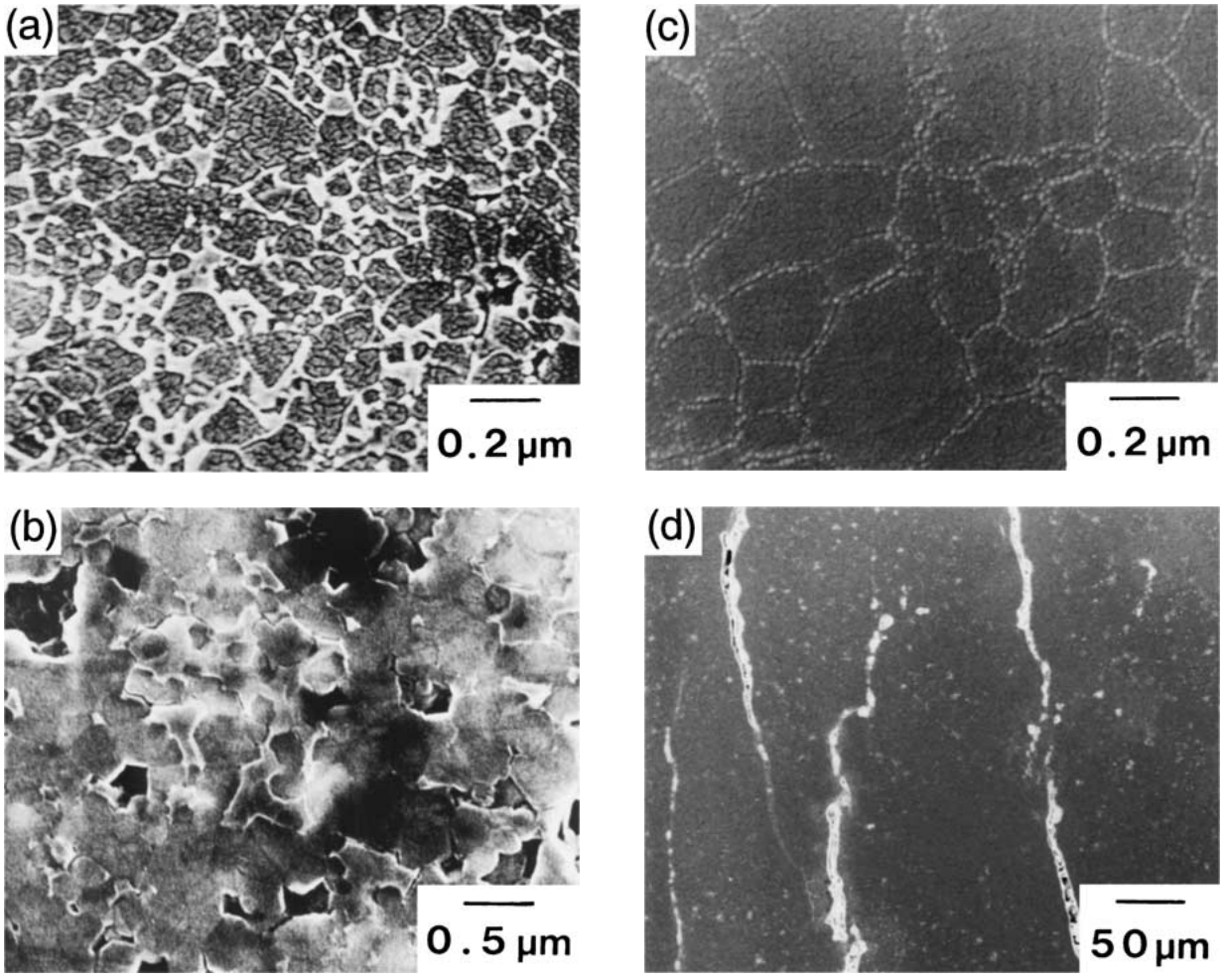

Figure 3 Microstructure of (a) as-sintered SiC, (b) after tensile deformation in Ar (2023 K, 2E-4 s^{-1}, 50% elongation, tensile axis is horizontal), (c) after tensile deformation in N_2 (×50 K, 2023 K, 5E-5 s^{-1}, 7.3% elongation, tensile axis is horizontal) and (d) after tensile deformation in N_2 (×100, 2023 K, 5E-5 s^{-1}, 7.3% elongation, tensile axis is horizontal).

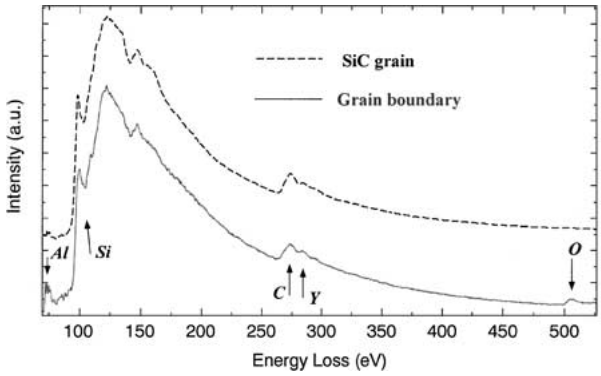

Figure 5 ELNES results for Al-L edges, Si-L edges, Y-M edge, C-K edge, and O-K edge at grain and grain boundary in as-sintered material.

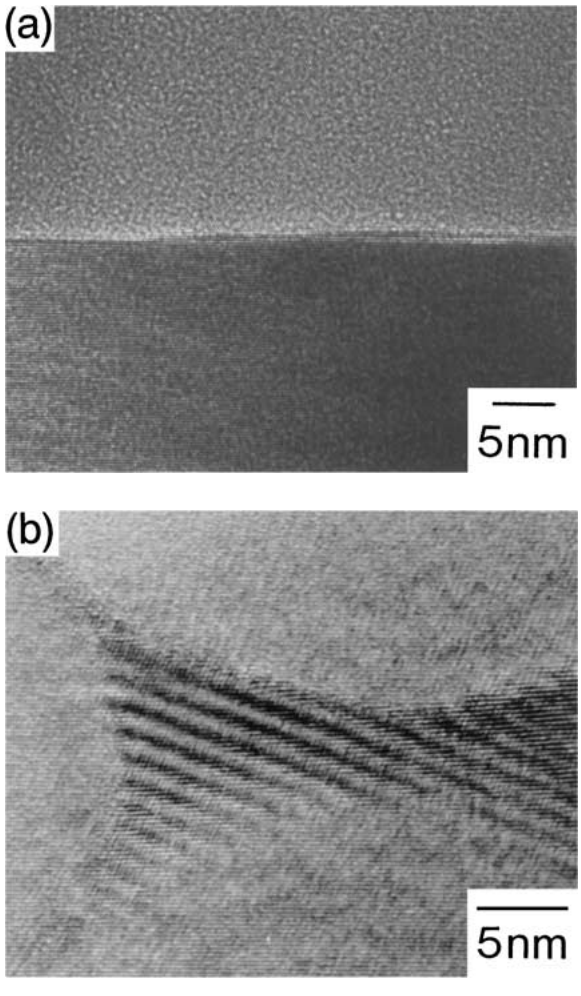

Figure 6 High-resolution TEM image at grain boundaries after (a) tensile deformation in Ar (1998 K, 5E-5 s^{-1}, 60% elongation) and (b) tensile deformation in N_2 (1998 K, 5E-5 s^{-1}, 5.0% elongation).

in the SiC spectrum. The grain-boundary spectrum also reveals that the amorphous layer contained silicon and carbon segregation that was detected in the SiC spectrum. Although signals from Si and C probably originated from the bulk grain, silicon carbide, a Si-Al-Y-O glass is expected at the grain boundaries judging from the ELNES results.

HRTEM images of the grain boundary in deformed samples in both argon and N_2 are shown in Fig. 6. In samples deformed in argon, the amorphous phase was difficult to observe in most of grain boundaries

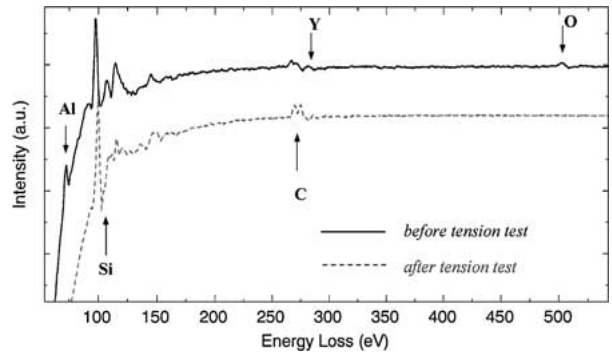

Figure 7 ELNES results for Al-L edges, Si-L edges, Y-M edge, C-K edge, and O-K edge at grain boundary after tensile deformation in Ar (1998 K, 5E-5 s^{-1}, 60% elongation).

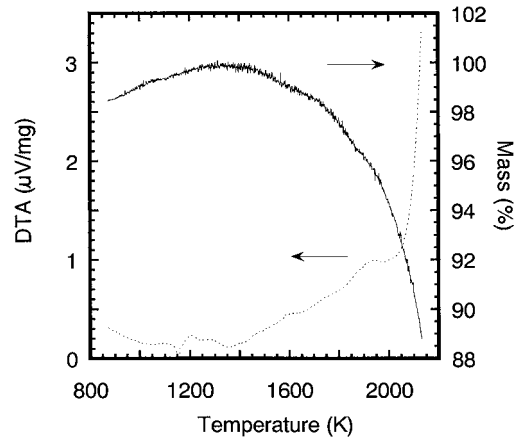

Figure 8 TG-DTA curves of as-sintered SiC in Ar.

as shown in Fig. 6a. In samples deformed in N_2, a crystalline phase was observed at many triple points and multi grain junctions. EDX results showed that this crystalline phase contained aluminum and nitrogen.

ELNES results for grain boundaries before and after tension tests in argon are shown in Fig. 7. The peaks for aluminum and oxygen have completely disappeared and that of yttrium has almost disappeared after tensile deformation in argon.

3.3. TG-DTA analysis

TG-DTA curves in argon are shown in Fig. 8. The increasing of weight loss at the temperature range from room temperature to 1300 K was originated from residual gas in the furnace. Weight loss began about 1300 K and showed about 6% at 2000 K. The endothermic reaction suddenly increased at about 2000 K.

3.4. XRD analysis

The crystalline phase of the as-sintered material was a β-SiC(3C) single phase. No phase transformation from β to α was detected after deformation in either argon or N_2 atmospheres. Amounts of the crystalline phase at triple points and multi grain junctions in the sample deformed in N_2 were below the detection limit.

4. Discussion

In deformed samples, no phase transformation or multiplication of dislocation were found. The SiC grains retained their equiaxed shape, when grain growth occurred during large deformation. Therefore,

TABLE I Results of tension tests

Atmosphere	Temperature (K)	Strain rate (s^{-1})	Elongation (%)	Weight loss (%)
Ar	1973	5×10^{-5}	39	11.8
	1998	5×10^{-5}	60	11.2
	2048	5×10^{-5}	44	12.0
N_2	1998	5×10^{-5}	5.0	4.7
	2023	5×10^{-5}	7.3	4.8

grain-boundary sliding is identified as the major mechanism of deformation in this material. The amorphous films at the grain boundaries became liquid at temperatures higher than the glass-transition temperature and also could be a supercooled liquid below that temperature. Such films were beneficial to deformation at high temperature. Authors of this work reported that SiC with the addition of Al showed rapid strain hardening by the vaporization of grain-boundary phase during tension test [15].

4.1. Ar atmosphere

The plateau region which specimen deformed at constant stress was obtained in Fig. 1. In this region, the deformation is thought to be enhanced by the amorphous phase. The weight loss during tension tests (11–12 wt%) was higher than the weight of sintering additive as shown in Table I. Therefore, the decomposition of SiC was thought to be occurring concurrently with the vaporization of the grain-boundary phase.

An oxide layer is formed on the surface of the raw SiC powder, in addition to the oxides used as sintering additives. This adsorbed oxygen remains within the sintered body and reacts with SiC at temperatures greater than 1573 K and decomposes the SiC as follows [16].

$$SiC(s) + 2SiO_2(1) \rightarrow 3SiO(g) \uparrow + CO(g) \uparrow \quad (4)$$

In the Al_2O_3-Y_2O_3 system, the decomposition of SiC and the vaporization of additives occur at the same time at >1973 K [16].

$$SiC(s) + Al_2O_3(s) \rightarrow Al_2O(g) \uparrow + SiO(g) \uparrow + CO(g) \uparrow \quad (5)$$

$$SiC(s) + Y_2O_3(s) \rightarrow Y_2O(g) \uparrow + SiO(g) \uparrow + CO(g) \uparrow \quad (6)$$

Grande and co-workers investigated the evaporation of liquid-phase sintered SiC during sintering by thermogravimetry in a graphite furnace. They reported that the amount of yttrium-containing secondary phase did not significantly reduce during heat treatment at 2093 K for 6 h. However, in our experiment at the temperature range from 1973 K to 2023 K, amorphous phase was partially remained at the grain boundaries. Therefore, the occurrence of cavitation at triple points during superplastic deformation may enhance the vaporization of grain-boundary phase.

It is obvious that the presence of oxygen is one of the origins for the decomposition of SiC and the vaporization of sintering additives. Therefore, the weight-loss can be affected by the total amount of oxygen content, basically the amount of the oxygen impurity, that of the oxide additives and oxygen partial pressure (Po_2).

In this atmosphere, the deformation temperature should be lower than 1973 K to suppress the vaporization of grain-boundary phase and the decomposition of SiC. The samples, however, exhibited only 16% elongation at the initial strain rate of $2 \times 10^{-5}\ s^{-1}$ at 1873 K.

4.2. N_2 atmosphere

Dissolved nitrogen inhibits the atomic transport processes responsible for sintering of SiC [12, 17]. For thermal decomposition and vaporization as in the present case, however, reaction at the interfaces between SiC grains and secondary phases would be a dominant mechanism rather than the diffusion or mass transport of chemical species. Originally, the crystallization of grain-boundary phase was considered to be preventing weight-loss. The heat treatment in N_2 suppressed the vaporization and decomposition of grain-boundary phase, and promoted nitrogen substitution within grain-boundary phase. Nitrogen can dissolve in silica or aluminosilicate glasses physically or chemically [18]. Although physical solubility in aluminosilicates is considered to be small [19], it may cause of the increase in weight as well as the dissolution of nitrogen into SiC. In the case of chemical dissolution, on the other hand, nitrogen dissolution proceeds by the substitution of oxygen ions into nitrogen in the network structure. According to Hwang *et al.* [19] chemical dissolution of nitrogen in oxynitride melts takes place as following reaction when the oxidation reaction of SiC is involved:

$$N_2 + SiC + (O) \rightarrow 2(N) + (Si) + CO \uparrow \quad (7)$$

where the parentheses in the equation indicate solution in the melts. The reaction indicates the conversion of (SiO_2) in the Al-Si-O glass to (Si_3N_4) according to the reaction.

$$2N_2 + 2SiC + (SiO_2) \rightarrow (Si_3N_4) + 2CO \uparrow \quad (8)$$

Similarly, formation reaction of AlN can be written as

$$2N_2 + 3SiC + (2Al_2O_3) \rightarrow (4AlN) + 3SiO \uparrow + 3CO \uparrow \quad (9)$$

or

$$3N_2 + 3SiC + (Al_2O_3) \rightarrow (2AlN) + (Si_3N_4) + 3CO \uparrow \quad (10)$$

Elongation in N_2 atmosphere was always <8% at the different strain rates. Such brittle fracture was a result of the inhibition of grain-boundary sliding by crystallization of the grain-boundary phase. However, as we reported previously [11], and N_2 atmosphere has the advantage over an argon atmosphere for suppressing vaporization of the grain-boundary phase and the decomposition of SiC. Weight loss during testing in N_2 was about 5% as shown in Table I. Therefore, the amorphous phase, which is stable in an N_2 atmosphere, is very important for achieving even larger deformation in liquid-phase-sintered SiC.

5. Conclusions

Tension tests were conducted on liquid-phase-sintered SiC with additions of 5.135 wt% Al_2O_3 and 3.867 wt% Y_2O_3 using a universal testing machine at constant crosshead speeds, with initial strain rates between 3×10^{-4} and 2×10^{-5} s^{-1} and at temperatures between 1873 and 2048 K in both argon and N_2 atmospheres.

In argon atmosphere, it was observed that:

1. Maximum tensile elongation reached 60% at an initial strain rate of 5×10^{-5} s^{-1}, at 1998 K.

2. No phase transformation or multiplication of dislocation were observed in deformed samples.

3. The vaporization of grain-boundary phase and grain growth during tests prevented further elongation.

In N_2 atmosphere, it was observed that:

4. A cry stalline phase was formed at the triple points and multi grain junctions during tension tests; consequently, the samples exhibited brittle fracture.

5. No phase transformation or multiplication of dislocation were observed in deformed samples.

6. The cracks were propagated in the vertical direction of tensile axis in deformed samples.

These results showed that the major deformation mechanism in the present study was grain-boundary sliding.

References

1. S. PROCHAZKA, Special Ceramics 6, edited by P. Popper (British Ceramic Research Association, Stoke-on-Trent, 1975) p. 171.
2. K. SUZUKI, *Rep. Res. Lab., Asahi Glass Co., Ltd.* **36** (1986) 25.
3. M. OMORI and H. TAKEI, *J. Amer. Ceram. Soc.* **65** (1982) C-92.
4. M. MITOMO, Y.-W. KIM and H. HIROTSURU, *J. Mater. Res.* **11** (1996) 1601.
5. T. NAGANO, S. HONDA, F. WAKAI and M. MITOMO, in Proc. of 6th Int'l Symp. on Ceramic Materials and Components for Engines, Arita, October 1997, edited by K. Niihara, S. Hirano, S. Kanzaki, K. Komeya and K. Morinaga (Japan Fine Ceramics Association, Tokyo, 1998) p. 707.
6. *Idem.*, in Proc. of Superplasticity & Superplastic Forming 1998, San Antonio, February 1998, edited by A. K. Ghosh and T. R. Bieler (The Minerals, Metals & Materials Society, Warrendale, 1998) p. 247.
7. T. NAGANO, H. GU, K. KANEKO, G.-D. ZHAN and M. MITOMO, *J. Amer. Ceram. Soc.* **84** (2001) 2045.
8. T. NAGANO, H. GU, Y. SHINODA, M. MITOMO and F. WAKAI, Ceramics: Getting into The 2000's, Part D, Florence, June 1998, edited by P. Vincenzini (Techna, Faenza, 1999) p. 25.
9. T. NAGANO, H. GU, Y. SHINODA, G.-D. ZHAN, M. MITOMO and F. WAKAI, *Mater. Sci. Forum* **304/306** (1999) 507.
10. N. KONDO, F. WAKAI, M. YAMAGIWA, T. NISHIOKA and A. YAMAKAWA, *Material Science and Engineering* A **A206** (1996) 45.
11. T. NAGANO, K. KANEKO, G.-D. ZHAN and M. MITOMO, *J. Amer. Ceram. Soc.* **83** (2000) 2781.
12. H.-W. JUN, H.-W. LEE, G.-H. KIM, H. SONG and B.-H. KIM, *Ceram. Eng. Sci. Proc.* **18** (1997) 487.
13. I. D. PRENDERGAST, D. W. BUDWORTH and N. H. BRETT, *Trans. Brit. Ceram. Soc.* **71** (1972) 31.
14. H. TANAKA and N. IYI, *J. Ceram. Soc. Jpn.* **101** (1993) 1313.
15. T. NAGANO, K. KANEKO and H. KODAMA, in Proc. of The Third Pacific Rim Int'l Conference on Advanced Materials and Processing (PRICM3), edited by M. A. Imam, R. DeNale, S. Hanada, Z. Zhong and D. N. Lee (The Minerals, Metals & Materials Society, Warrendale, 1998) p. 1897.
16. T. GRANDE, H. SOMMERSET, E. HAGEN, K. WIIK and M.-A. EINARSRUD, *J. Amer. Ceram. Soc.* **80** (1997) 1047.
17. W.-S. SEO, C.-H. PAI, K. KOUMOTO and H. YANAGIDA, *J. Ceram. Soc. Japan* **99** (1991) 443.
18. H. O. MULFINGER, *J. Amer. Ceram. Soc.* **49** (1966) 462.
19. S.-L. HWANG, P. F. BECHER and H.-T. LIN, *ibid.* **80** (1997) 329.

Received 25 October 2001
and accepted 20 June 2002